## Cascade of Multielectron Bubble Phases in Monolayer Graphene at High Landau Level Filling

Fangyuan Yang,<sup>1</sup> Ruiheng Bai<sup>®</sup>,<sup>1</sup> Alexander A. Zibrov,<sup>1</sup> Sandeep Joy<sup>®</sup>,<sup>2</sup> Takashi Taniguchi,<sup>3</sup> Kenji Watanabe<sup>®</sup>,<sup>3</sup> Brian Skinner<sup>®</sup>,<sup>2</sup> Mark O. Goerbig,<sup>4</sup> and Andrea F. Young<sup>®</sup>,<sup>1</sup>\*

<sup>1</sup>Department of Physics, University of California at Santa Barbara, Santa Barbara, California 93106, USA

<sup>2</sup>Department of Physics, Ohio State University, Columbus, Ohio 43210, USA

<sup>3</sup>National Institute for Materials Science, 1-1 Namiki, Tsukuba 305-0044, Japan

<sup>4</sup>Laboratoire de Physique des Solides, CNRS UMR 8502, Université Paris-Saclay, 91405 Orsay Cedex, France

(Received 7 September 2023; accepted 23 October 2023; published 27 November 2023)

The phase diagram of an interacting two-dimensional electron system in a high magnetic field is enriched by the varying form of the effective Coulomb interaction, which depends strongly on the Landau level index. While the fractional quantum Hall states that dominate in the lower-energy Landau levels have been explored experimentally in a variety of two-dimensional systems, much less work has been done to explore electron solids owing to their subtle transport signatures and extreme sensitivity to disorder. Here, we use chemical potential measurements to map the phase diagram of electron solid states in N=2, N=3, and N=4 Landau levels in monolayer graphene. Direct comparison between our data and theoretical calculations reveals a cascade of density-tuned phase transitions between electron bubble phases up to two, three, or four electrons per bubble in the N=2, 3, and 4 Landau levels, respectively. Finite-temperature measurements are consistent with melting of the solids for  $T\approx 1$  K.

DOI: 10.1103/PhysRevLett.131.226501

In an electron solid, spatial translation symmetry is spontaneously broken so that the ground state charge density forms a periodic structure incommensurate with the underlying crystal lattice. One known example is obtained in high Landau levels (LLs) in two-dimensional (2D) electron systems. Theoretically, the phase diagram is expected to host a rich interplay of competing phases [1–9]. A unique feature of electron solids in higher LLs is that a variable number of electrons may cluster on each site of the emergent crystal. The formation of the phases—known as "electron bubbles"—is driven by the structure of the electronic form factors in the LLs. Electron bubble phases were predicted theoretically [1–4] and first identified in the GaAs 2D electron gas by the observation of the reentrant integer quantum Hall effect (RIQHE) in transport measurement [10,11], in which the crystallized electrons freeze and no longer contribute to the Hall conductivity. Similar phases are also expected in graphene [12-14], and recent measurements have confirmed their existence [15,16]. While the existence of electron solids is straightforward to confirm using transport measurements, distinguishing them from each other to construct a comprehensive phase diagram is not. To this end, other experimental methods, such as microwave spectroscopy [17], surface acoustic wave transmission [18,19], and tunneling spectroscopy [20], have been developed to study vibrating modes related to the lattice structure of electron solids. More recently, temperature-dependent transport has shown that the same RIOH state may host more than one bubble phase, distinguished by different melting temperatures [21–23]. However, a detailed phase diagram of the electron bubble phases across different LLs, long predicted by theory, has not been conclusively established.

Measuring thermodynamic properties provides a probe of quantities directly related to the ground state energy, offering a chance to map out a complete phase diagram independent of the detailed transport phenomenology of the ground state. In this Letter, we use chemical potential measurements [24] to construct just such a phase diagram for partially filled LLs in monolayer graphene. Our data demonstrate the existence of multiple distinct electron bubble phases characterized by different bubble sizes. By directly comparing our data with mean-field-theory calculations, we establish a one-to-one correlation between the filling factor and the electron bubble morphology.

Our measurement is performed in a graphene/h-BN heterostructure assembled using standard dry pickup techniques [25]. Two graphene monolayers are separated by an h-BN dielectric layer of 40 nm thickness, with additional h-BN dielectric and graphite gates forming a four-plate capacitor geometry. The top graphene serves as a charge detector, which combined with a feedback loop allows us to determine changes in chemical potential of the bottom "sample" graphene accurately [24].

Figure 1 presents the chemical potential  $\mu$  measured across individual LLs with orbital quantum numbers N=0,1,2,3, and 4 on the hole carrier side. The chemical potential is plot as a function of the effective filling factor,

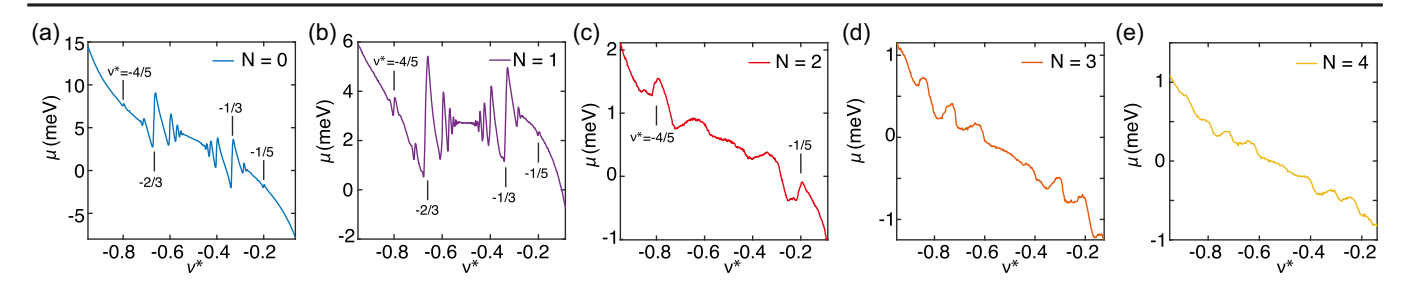


FIG. 1. Fractional quantum Hall (FQH) and electron solid states in graphene monolayer probed by chemical potential measurements. (a) Chemical potential change as a function of effective filling factor,  $\nu^* \equiv \nu - \lceil \nu \rceil$ , in the N=0, (b) N=1, (c) N=2, (d) N=3, and (e) N=4 LLs. In the N=0 and N=1 LLs, FQH states are observed as jumps in  $\nu$  at  $\nu^*=p/(2p\pm 1)$  and  $\nu^*=p/(4p\pm 1)$  ( $p=1,2,3,\ldots$ ), a selection of which are labeled. For  $N\geq 2$ , broad oscillatory features dominate, which we associated with electron solids. The N=2 LL is a marginal case where fractional quantum Hall states and electron bubbles compete within a narrow range of filling factors. All data measured at B=13 T and T=15 mK.

 $\nu^* \equiv \nu - \lceil \nu \rceil$ , where  $\nu$  is the actual filling factor and  $\lceil \nu \rceil$  is the integer part of the filling factor. The qualitative behavior of  $\mu$  depends strongly on N. For N=0 and N=1 [Figs. 1(a) and 1(b)], fractional quantum Hall states are favored, with incompressible states (manifesting here as nearly discontinuous jumps in  $\mu$ ) observed at filling factors associated with two-flux and four-flux composite fermion sequences [26]. For  $\nu^* > -1/5$  (or  $\nu^* < -4/5$ ) within the N=0 and N=1 LL,  $\mu$  changes smoothly, showing a large negative inverse compressibility  $d\mu/d\nu$  [27]. This behavior has been identified with the formation of Wigner crystal states in previous experiments in both GaAs [28,29] and graphene [24,30].

For  $N \ge 2$  [Figs. 1(c)–1(e)], a qualitatively different behavior is observed, with  $\mu$  dominated by much weaker oscillatory features that are not associated with any particular fractional  $\nu$ . As we elaborate upon below, these features are signatures of multielectron bubble states. Bubble states are generically expected in higher LLs due to the nature of the single-particle wave functions, which feature multiple nodes. This form factor considerably modifies the Coulomb repulsion at short distances, favoring charge-density-wave-type states instead of incompressible fractional quantum Hall states. In the N=2 LL, our measurement reveals a competition between the FQH states observed at  $\nu^* = -1/5$  and -4/5 and electron bubble states, as reported previously [15]. In the N=3 and N=4LLs, the electron bubble phases are favored over the entire range of filling factors, manifesting as a slow modulation of  $\mu$  and  $d\mu/d\nu$ , as shown in Figs. 2(a) and 2(b). The number of oscillatory features increases with N. In the N=3 and N = 4 LL, we observed three and four pairs of features, related by particle hole symmetry about  $\nu^* = -1/2$ , respectively.

The panels in Figs. 2(a) and 2(b) show  $d\mu/d\nu$  measured over a range spanning several LLs each, grouped by their orbital quantum number. For the N=3 orbital [Fig. 2(a)], the four curves depicted are acquired in filling factor ranges corresponding to each of the four symmetry-broken levels spanning  $-10 < \nu < -6$ . Because of limitations on the

range of the electrostatic gates, for the N=4 LL [Fig. 2(b)] only  $-12 < \nu < -10$  is shown. Remarkably, the repetition of the pattern of  $\mu$  oscillations across different symmetry-broken levels indicates that this physics is independent of the spin and valley order. We may conclude that the formation of the bubble phases is governed only by single-component LL physics; as a consequence, the

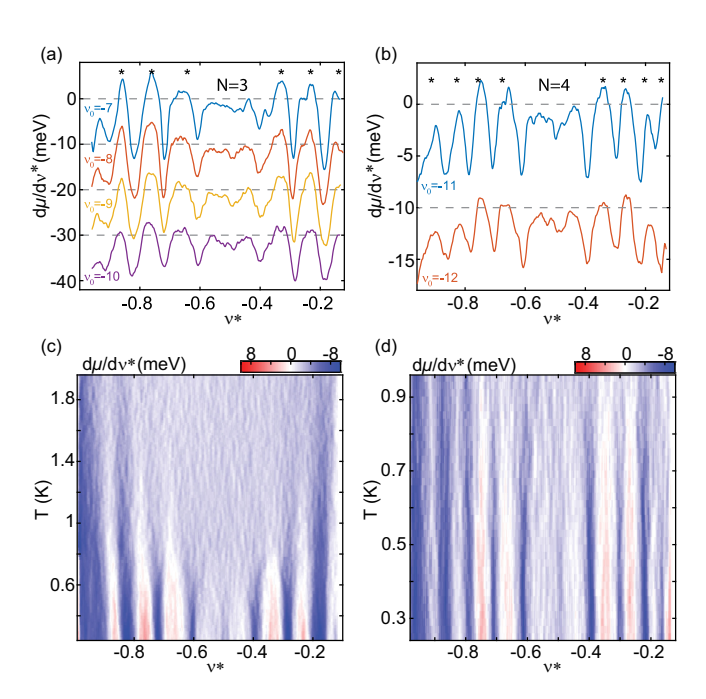


FIG. 2. Electronic compressibility and temperature dependence of electron bubble phases. (a)  $d\mu/d\nu^*$  in the N=3 and (b) N=4 LLs. The data are obtained via numerical differentiation of  $\mu$  measured at 13 T and 15 mK. Within each LL, the four symmetry-breaking levels are plotted by blue, red, orange, and purple curves with increasing  $|\nu|$ .  $\nu_0$  represents the actual integer filling factor on the left side of each level. The curves are offset as indicated by the gray dashed lines. Stars indicate the center of the regions identified with electron bubble states. (c) Temperature dependence of electron bubble states in N=3 and (d) N=4 LLs, measured at B=13 T.

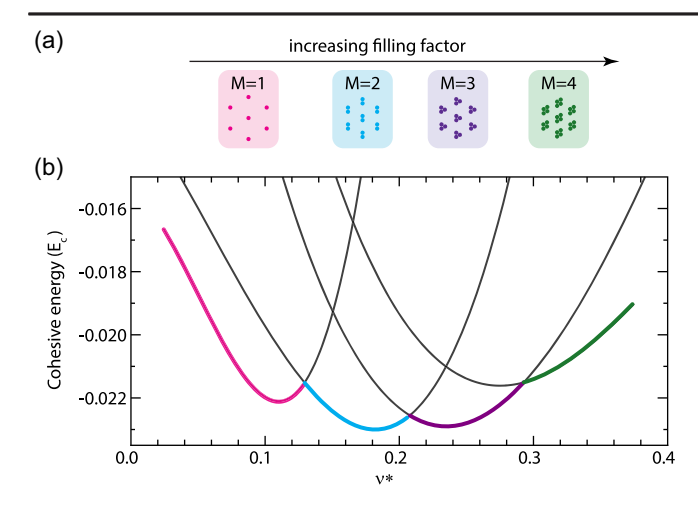


FIG. 3. Cohesive energy for electron bubble states. (a) Schematic depiction of electron bubble phases in the N=4 LL. (b) Calculated cohesive energy for the N=4 LL (see Supplemental Material [33] for details). The ground state is obtained by tracing the lowest-energy state at each filling factor, which is highlighted by colored lines. The color codes here match those in panel (a).

bubbles are not expected to be accompanied by complex spin or valley textures as have been shown to play a role in lower LLs [30,31].

The energy scale characterizing the bubble phases may be directly accessed via the temperature dependence, shown in Figs. 2(c) and 2(d). Signatures of the bubble phases disappear rapidly for  $T \approx 1-2$  K in the N = 3 LL and below 1 K in the N = 4. This is consistent with the general scale of the chemical potential changes associated with these phases, which are on the order of a few hundred μeV, as well as previously reported transport data [15]. The order of magnitude of this scale is consistent with simplified Lindemann criterion [32] for crystal melting, according to which the thermal position fluctuations need to be roughly 15% of the lattice spacing to make the crystal melt. Within the harmonic approximation for the crystal, one obtains critical temperatures in the  $\sim 1$  K range (see Supplemental Material [33]). Notably, the energy scale of the bubble phases is considerably smaller than that of the fractional quantum Hall physics in the lower LLs, where gaps (at comparable magnetic fields) typically are in the > 10 K range.

Theoretically, the ground state of the interacting electron system in a partially filled high-N Landau level is expected to evolve through a series of multielectron bubble phases, as illustrated in Fig. 3(a) for the case of N=4. These crystalline phases can be described within a mean-field approach as presented in detail in Supplemental Material [33]. Figure 3(a) shows the cohesive energy per particle for the bubble crystals with M electrons per lattice site as a function of the effective filling factor  $\nu^*$  [4]. The cohesive energy is the energy per particle, from which we have

already subtracted the Hartree-Fock energy of a featureless electronic liquid [9] as well as the charging energy of the parallel plate capacitor in which the sample is embedded. For a fixed value of M, the energy of the triangular bubble crystals depends on the spacing  $\Lambda_B = \sqrt{4\pi M/\sqrt{3}\nu^* l_B}$  between the bubbles, which, in turn, depends on the effective filling  $\nu^*$ . Here,  $l_B = \sqrt{\hbar/eB}$  is the magnetic length.

One obtains a family of curves, with minima at positions described approximately by  $\nu^* \sim M/2N$ . The M-bubble phase is realized whenever it is lowest in energy within a certain filling-factor range. Within a given Landau level, the maximum stabilized value of M equals N [2]. Theoretically, one may even stabilize a bubble phase with M = N + 1 in the vicinity of a half-filled, singly degenerate Landau level ( $\nu^* \sim 1/2$ ) [8]. However, this phase is thought to compete energetically with a stripe phase; we find no evidence for it in the experimental data.

Notably, the family of minimum energy curves shown in Fig. 3(b) are not convex upon variation of  $\nu^*$ , a signature of thermodynamic instability to the formation of mixed phases in which parts of the sample area are occupied by crystals with differing number of electrons per bubble. However, we note that, for our experimental geometry, the variations in internal energy caused by the bubble phases are dwarfed by the electrostatic energy of the electron gas. Taking this into account, mixed phases are found only in a range  $\delta\nu\approx 2\times 10^{-3}$  (see Supplemental Material [33]) in the vicinity of the level crossings visible in Fig. 3(b). In this picture, then, we expect a succession of pure bubble phases, separated by sharp phase transitions.

To facilitate comparison between experiment and theory, in Figs. 4(a)–4(c), we plot the experimentally measured  $\mu$ scaled by the Coulomb energy,  $E_c=e^2/(\epsilon\ell_B)$  . Each panel presents  $\mu$  measured at different values of the magnetic field B for the same LL fillings, with an offset of  $0.01E_C$ between curves introduced for clarity. The  $\mu$  modulations observed in the curves are almost identical in these units, as expected given the Coulomb-driven nature of the electron bubble phases. Figures 4(d)-4(f) present the calculated chemical potential of electron bubble phases in the N=2, N = 3, and N = 4 LLs in the absence of disorder. The solid curves are obtained from the calculated energy per particle E of the M-bubble phases via  $\mu = \partial(\nu E)/\partial\nu$  [9]. Note that, in these calculations, we restore the contribution of the featureless background charge omitted above in the calculation of the cohesive energy. Our calculations account for screening caused by both the dielectric environment as well as inter-Landau level excitations in the graphene [38,39]. As in the N=0 and N=1 Landau levels [24], accurately accounting for screening is required for quantitative agreement between experiment and theory in graphene.

Despite the comparative simplicity of our model, it agrees quantitatively with the data in the overall scale of

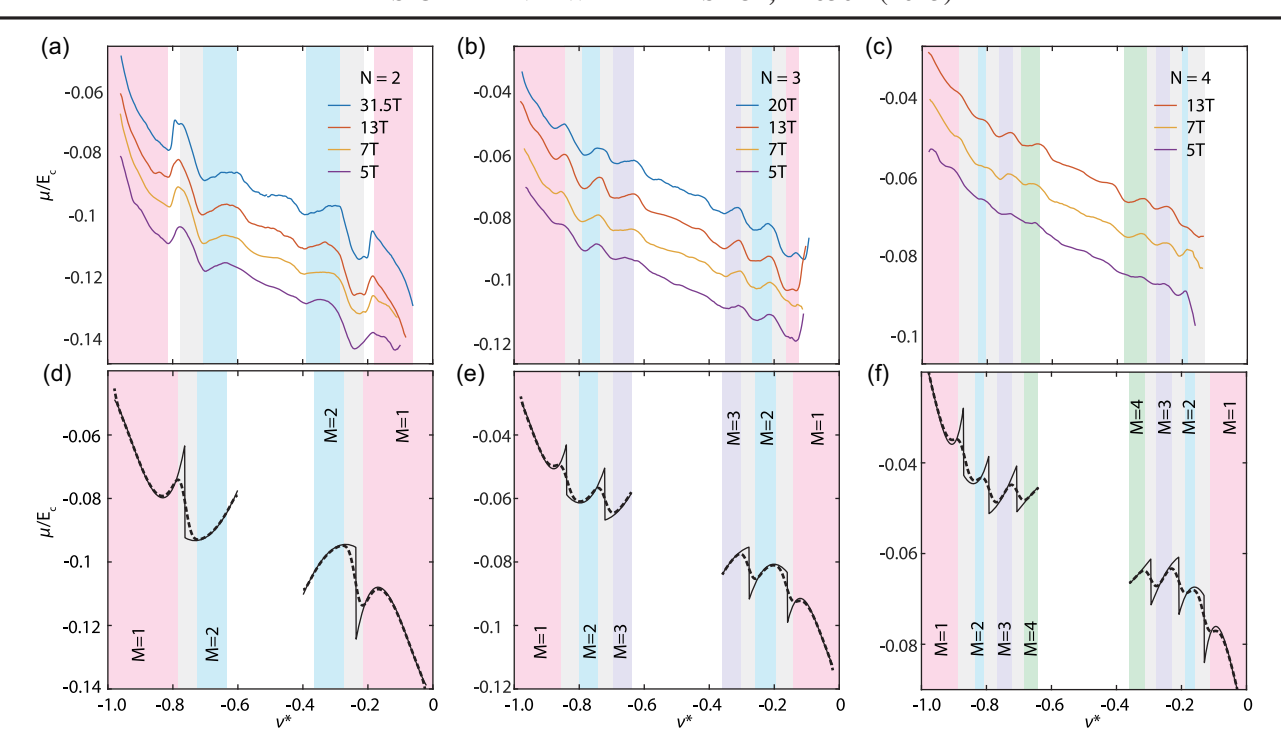


FIG. 4. Quantitative comparison with theoretical model of electron bubble cascade. (a)  $\mu(\nu^*)$  at several magnetic fields in the N=2, (b) N=3, and (c) N=4 Landau level. The data at B=31.5 and 20 T were measured at 300 mK, while the data at 13, 7, and 5 T were measured at 15 mK. The chemical potential change is presented in units of the Coulomb energy  $E_c=(e^2/\epsilon l_B)\approx 12.5$  meV  $\cdot \sqrt{B/T}$ . The red, orange, and purple curves are offset by  $-0.01E_c$ ,  $-0.02E_c$ , and  $-0.03E_c$  from the blue curve, respectively. (d) Chemical potential calculated by mean field theory (solid lines; see Supplemental Material [33]) in the N=2, (e) N=3, and (f) N=4 Landau level. The dashed lines in these panels are chemical potential taking disorder broadening into account. The pink, blue, purple, and green color bars represent the domain of stability for the M=1, M=2, M=3, and M=4 electron bubble phases within the disorder broadened model, respectively. The gray regions represent broadened phase transitions where neighboring pure electron bubble phases coexist. Panels (a)–(c) use the same color codes to label the corresponding regions identified by experiments from the sign of the compressibility.

the chemical potential modulation across the Landau level, as well as in the locations of the various bubble phases, which we identify with positive compressibility regions for the  $M \ge 2$ . However, in contrast to the theoretical model, where the phase transitions are sharp, in the experimental data the phase transitions are marked by broad regions of negative compressibility typically rather than sharp jumps. It is natural to associate these regions with a mixed phase arising from disorder potentials. To capture this physics, we convolve the disorder-free curves with a Gaussian "inhomogenous broadening" of width  $\Delta \nu = 0.015$  at 13 T. Given the negligible quantum capacitance in the bubble regime, this is equivalent to an energy broadening  $\Delta E = 7.5$  meV. The dashed curves in Figs. 4(d)-4(f) show the results of this model. We use the same color code to label the regions associated with pure and mixed electron bubble phases in both experimental and simulation data in the figure; the disordered model quantitatively reproduces the key missing feature of the experimental data, replacing the cusps of the disorder-free model with negative compressibility regimes as observed experimentally.

We note in closing several open questions raised by our work. First, while electron solids evidently dominate the ground states for N > 2, it is likely that they appear in the lower LLs as well but are difficult to detect with bulk methods where their subtle thermodynamic or transport phenomenology may be overwhelmed by the incompressibility of the fractional quantum Hall states. Second, it is unclear whether the particular orbital wave functions of single- and multilayer graphene may lead to any particularities in the electron solid ground states as compared to semiconductor systems. Finally, our disorder model is likely to be gross oversimplification. In particular, the lack of observed magnetic field dependence in the sharpness of the phase transitions is at odds with a model of quenched disorder where the effective broadening  $\Delta E$  would be expected to be magnet field independent. These and other questions might be directly resolved via scanning tunneling microscopy measurements of the real space structure of these phases [31,40], as well as more detailed theoretical modeling that accounts for the interplay of disorder, finite temperature, and mesoscopic phase separation.

The authors acknowledge discussions with M. Zaletel and B. Shklovskii. This work was primarily supported by Office of Naval Research under Grant No. N00014-23-1-2066. A. F. Y. acknowledges the additional support of the Gordon and Betty Moore Foundation Emergent Phenomena in Quantum Systems Initiative program under Grant No. GBMF9471. A portion of this work was performed at the National High Magnetic Field Laboratory, which is supported by National Science Foundation Cooperative Agreement No. DMR-1644779 and the State of Florida. This work made use of shared facilities supported by the National Science Foundation through Enabling Quantum Leap: Convergent Accelerated Discovery Foundries for Quantum Materials Science, Engineering and Information (Q-AMASE-i) Grant No. DMR-1906325. K. W. and T. T. acknowledge support from JSPS KAKENHI (Grants No. 19H05790, No. 20H00354, and No. 21H05233). S. J. and B. S. were supported by the NSF under Grant No. DMR-2045742.

- \*andrea@physics.ucsb.edu
- [1] A. A. Koulakov, M. M. Fogler, and B. I. Shklovskii, Phys. Rev. Lett. **76**, 499 (1996).
- [2] M. M. Fogler, A. A. Koulakov, and B. I. Shklovskii, Phys. Rev. B 54, 1853 (1996).
- [3] R. Moessner and J. T. Chalker, Phys. Rev. B 54, 5006 (1996).
- [4] M. M. Fogler and A. A. Koulakov, Phys. Rev. B 55, 9326 (1997).
- [5] F. D. M. Haldane, E. H. Rezayi, and K. Yang, Phys. Rev. Lett. 85, 5396 (2000).
- [6] N. Shibata and D. Yoshioka, Phys. Rev. Lett. 86, 5755 (2001).
- [7] M. M. Fogler, in *High Magnetic Fields*, edited by R. Beig *et al.* (Springer, Berlin, 2002), Vol. 595, pp. 98–138.
- [8] R. Côté, C. B. Doiron, J. Bourassa, and H. A. Fertig, Phys. Rev. B **68**, 155327 (2003).
- [9] M. O. Goerbig, P. Lederer, and C. M. Smith, Phys. Rev. B **69**, 115327 (2004).
- [10] M. P. Lilly, K. B. Cooper, J. P. Eisenstein, L. N. Pfeiffer, and K. W. West, Phys. Rev. Lett. 82, 394 (1999).
- [11] R. R. Du, D. C. Tsui, H. L. Stormer, L. N. Pfeiffer, K. W. Baldwin, and K. W. West, Solid State Commun. 109, 389 (1999).
- [12] Z. Papic, R. Thomale, and D. A. Abanin, Phys. Rev. Lett. 107, 176602 (2011).
- [13] M. E. Knoester, Z. Papić, and C. Morais Smith, Phys. Rev. B **93**, 155141 (2016).
- [14] C.-H. Zhang and Y. N. Joglekar, Phys. Rev. B **75**, 245414 (2007).
- [15] S. Chen, R. Ribeiro-Palau, K. Yang, K. Watanabe, T. Taniguchi, J. Hone, M. O. Goerbig, and C. R. Dean, Phys. Rev. Lett. **122**, 026802 (2019).
- [16] Y. Zeng, J. I. A. Li, S. A. Dietrich, O. M. Ghosh, K. Watanabe, T. Taniguchi, J. Hone, and C. R. Dean, Phys. Rev. Lett. 122, 137701 (2019).

- [17] R. M. Lewis, P. D. Ye, L. W. Engel, D. C. Tsui, L. N. Pfeiffer, and K. W. West, Phys. Rev. Lett. 89, 136804 (2002).
- [18] M. E. Msall and W. Dietsche, New J. Phys. **17**, 043042 (2015).
- [19] B. Friess, Y. Peng, B. Rosenow, F. von Oppen, V. Umansky, K. von Klitzing, and J. H. Smet, Nat. Phys. 13, 1124 (2017).
- [20] J. Jang, B. M. Hunt, L. N. Pfeiffer, K. W. West, and R. C. Ashoori, Nat. Phys. 13, 340 (2016).
- [21] D. Ro, N. Deng, J. D. Watson, M. J. Manfra, L. N. Pfeiffer, K. W. West, and G. A. Csáthy, Phys. Rev. B 99, 201111(R) (2019).
- [22] X. Fu, Q. Shi, M. A. Zudov, G. Gardner, J. Watson, and M. Manfra, Phys. Rev. B 99, 161402(R) (2019).
- [23] D. Ro, S. A. Myers, N. Deng, J. D. Watson, M. J. Manfra, L. N. Pfeiffer, K. W. West, and G. A. Csáthy, Phys. Rev. B 102, 115303 (2020).
- [24] F. Yang, A. A. Zibrov, R. Bai, T. Taniguchi, K. Watanabe, M. P. Zaletel, and A. F. Young, Phys. Rev. Lett. 126, 156802 (2021).
- [25] L. Wang, I. Meric, P. Y. Huang, Q. Gao, Y. Gao, H. Tran, T. Taniguchi, K. Watanabe, L. M. Campos, D. A. Muller, J. Guo, P. Kim, J. Hone, K. L. Shepard, and C. R. Dean, Science 342, 614 (2013).
- [26] J. K. Jain, Phys. Rev. Lett. 63, 199 (1989).
- [27] M. S. Bello, B. I. Shklovskii, E. I. Levin, and A. Efros, Sov. Phys. JETP 53, 822 (1981), http://jetp.ras.ru/cgi-bin/dn/ e\_053\_04\_0822.pdf.
- [28] J. P. Eisenstein, L. N. Pfeiffer, and K. W. West, Phys. Rev. Lett. 68, 674 (1992).
- [29] J. P. Eisenstein, L. N. Pfeiffer, and K. W. West, Phys. Rev. B 50, 1760 (1994).
- [30] H. Zhou, H. Polshyn, T. Taniguchi, K. Watanabe, and A. F. Young, Nat. Phys. **16**, 154 (2020).
- [31] X. Liu, G. Farahi, C.-L. Chiu, Z. Papic, K. Watanabe, T. Taniguchi, M. P. Zaletel, and A. Yazdani, Science 375, 321 (2022).
- [32] F. A. Lindemann, Phys. Z. 11, 609 (1910).
- [33] See Supplemental Material at http://link.aps.org/supplemental/10.1103/PhysRevLett.131.226501 for theoretical calculations in detail, which includes Refs. [34–37].
- [34] M. O. Goerbig, P. Lederer, and C. Morais Smith, Phys. Rev. Lett. 93, 216802 (2004).
- [35] B. Spivak and S. A. Kivelson, Phys. Rev. B **70**, 155114 (2004).
- [36] B. Spivak, S. V. Kravchenko, S. A. Kivelson, and X. P. A. Gao, Rev. Mod. Phys. 82, 1743 (2010).
- [37] C. Ortix, J. Lorenzana, and C. Di Castro, Phys. Rev. B 73, 245117 (2006).
- [38] K. Shizuya, Phys. Rev. B 75, 245417 (2007).
- [39] R. Roldán, M. O. Goerbig, and J.-N. Fuchs, Semicond. Sci. Technol. 25, 034005 (2010).
- [40] A. Coissard, D. Wander, H. Vignaud, A. G. Grushin, C. Repellin, K. Watanabe, T. Taniguchi, F. Gay, C. B. Winkelmann, H. Courtois, H. Sellier, and B. Sacépé, Nature (London) 605, 51 (2022).